Research Square

Preprints are preliminary reports that have not undergone peer review.
They should not be considered conclusive, used to inform clinical practice,
or referenced by the media as validated information.

Targeting the TNFα/TNFR1 axis alleviates the experimental acute pancreatitis

Yin Zhu

ndyfy01977@ncu.edu.cn

The First Affiliated Hospital of Nanchang University https://orcid.org/0000-0002-7561-2306

Nianshuang Li

The First Affiliated Hospital of Nanchang University

xiaoli xi

The First Affiliated Hospital of Nanchang University

Pan Zheng

The First Affiliated Hospital of Nanchang University

Xueyang Li

The First Affiliated Hospital of Nanchang

Yuman Ye

Nanchang University

Yaoyu Zou

The First Affiliated Hospital of Nanchang

Maobin Kuang

The First Affiliated Hospital of Nanchang

Dongni Fu

The First Affiliated Hospital of Nanchang

Jianhua Wan

The First Affiliated Hospital of Nanchang University

Cong He

The First Affiliated Hospital of Nanchang University

Nonghua Lu

The First Affiliated Hospital of Nanchang

Article

Keywords: TNFα, TNFR1, AP, scRNA-seq, pomalidomide, inflammation

Posted Date: November 25th, 2025

DOI: https://doi.org/10.21203/rs.3.rs-8003658/v1

License: This work is licensed under a Creative Commons Attribution 4.0 International License.
Read Full License

Additional Declarations: (Not answered)

Abstract

Objective: Acute pancreatitis (AP) is an inflammatory disorder of the pancreas that can lead to life-threatening systemic inflammation and multiple organ failure with high mortality. The binding of tumor necrosis factor α (TNFα) to its receptor TNFR1 is a key driver of inflammation. Here, we demonstrate that genetic ablation or pharmacological inhibition of TNFR1 alleviate AP through reprogramming the immune microenvironment.

Methods: Experimental AP models were established in both Wild-type (WT) and *Tnfr1*$^{-/-}$ mice using three distinct methods for cross validation: cerulein administration, pancreatic duct ligation (PDL), and L-arginine injection. The TNF/TNFR1 axis was pharmacologically inhibited by Pomalidomide, Infliximab and Necrostatin-1 to evaluate their therapeutic effects in AP. Single-cell RNA (scRNA) and bulk RNA sequencing were employed to investigate the underlying mechanisms.

Results: We found the hyperactivation of the TNF/TNFR1 axis in AP models by analyzing publicly available scRNA-seq dataset. TNFα and TNFR1 mRNA and protein levels were significantly upregulated across three distinct AP animal models. Notably, genetic ablation of *Tnfr1* in mice obviously diminished AP severity, characterized by reduced inflammatory cell infiltration and decreased tissue inflammation. ScRNA-seq analysis revealed an altered immune landscape in *Tnfr1*$^{-/-}$mice, featuring both deceased proportions of inflammatory cells and the emergence of unique inflammatory suppression myeloid and neutrophil subpopulations. Furthermore, Integrated bulk RNA analysis identified downregulation of interferon-related genes (*Ifi209*, *Marcksl1*, *Ifit3*, *Oas3*) in inflammatory cells of *Tnfr1*$^{-/-}$ mice. Pharmacological inhibition of the TNFα/TNFR1 axis using pomalidomide pretreatment similarly attenuated AP inflammation and significantly suppressed these interferon-associated genes. Notably, therapeutic administration of pomalidomide post-AP induction reproduced these protective effects, confirming the translational potential of targeting this signaling pathway.

Conclusions: This study demonstrates that TNFα/TNFR1 axis drives AP pathogenesis, with *Tnfr1* ablation significantly reducing inflammation. We identify pomalidomide as a novel therapeutic agent that effectively attenuates AP severity by inhibiting this pathway, offering promising clinical translation potential.

Introduction

Acute pancreatitis (AP) is a critical abdominal emergency commonly associated with etiological factors including alcohol consumption, biliary obstruction, and hyperlipidemia[1] . While mild AP cases typically exhibit self-limiting characteristics with spontaneous resolution within days, a subset progresses to severe acute pancreatitis (SAP)[2] . SAP patients develop life-threatening systemic complications due to uncontrolled inflammatory cascades, including systemic inflammatory response syndrome (SIRS), multiple organ dysfunction syndrome, and intestinal barrier failure, with significantly elevated mortality rates[3]. Inflammation represents the hallmark pathological feature of AP, where initial inflammatory

responses trigger acinar cell injury, subsequently exacerbating the inflammatory cascade through positive feedback mechanisms[4, 5]. Consequently, early intervention targeting inflammatory mediator suppression and blockade of inflammatory amplification pathways constitutes a crucial therapeutic strategy for AP management.

TNFα (tumor necrosis factor α) is a pivotal proinflammatory cytokine primarily secreted by activated immune cells, including macrophages and T cells. It plays a central role in inflammation, immune responses, and apoptosis[6, 7]. TNFα exerts its pleiotropic biological effects by engaging two distinct receptors: tumor necrosis factor receptor 1 (TNFR1) and TNFR2[8]. While TNFR1 is ubiquitously expressed on most nucleated cells, TNFR2 exhibits restricted distribution, being predominantly limited to specific cell types such as immune cells and endothelial cells[6]. The

/TNFR1 axis is widely distributed and harbors a conserved death domain (DD) motif, primarily driving proinflammatory and tissue-degenerative responses. In contrast, TNFR2 mediates localized homeostatic effects, including cell survival and tissue regeneration[9, 10].

TNFα/TNFR1 axis is mediated through context-dependent homotypic DD interactions between TNFR1 trimers and downstream signaling components. This signaling cascade can induce the formation of at least three distinct complexes. Complex I formation triggers NF-κB and MAPK/ERK kinase pathway activation, thereby modulating inflammatory responses and cell death to coordinate immune regulation[11-13]. In contrast, Complex IIa and IIb initiate apoptotic and necroptotic cell death respectively, eliminating damaged or infected cells to maintain tissue homeostasis[6, 14] . The dynamic interplay between Complex I and II signaling ultimately dictates cellular fate decisions[15]. Recent studies revealed that Helicobacter pylori's infection activates the TNFα/TNFR1 axis in mice, triggering robust NLRP3 inflammasome assembly. Subsequent inflammasome activation drives macrophage polarization toward the pro-inflammatory M1 phenotype, exacerbating gastric inflammation[16]. The TNFα/TNFR1 axis plays a pivotal role in rheumatoid arthritis (RA) pathogenesis. TNFα/TNFR1 inhibition shifts macrophage polarization toward the anti-inflammatory M2 phenotype[17], and therapeutic blockade of this axis shows remarkable efficacy in RA treatment[18].

While the TNFα/TNFR1 axis has been well-characterized in various inflammatory disorders, its role in AP remains largely unexplored beyond serving as a diagnostic biomarker. Clinical studies have consistently revealed significant elevation of serum TNF-α levels in AP patients[19, 20], with concentrations positively correlating with disease severity[21]. Our preliminary data further confirm robust activation of the TNFα/TNFR1 axis following AP onset. Building on these findings, this study seeks to unravel the mechanistic basis of TNFα/TNFR1 axis in AP pathogenesis. Specifically, we will utilize *Tnfr1*$^{-/-}$ murine models to systematically study how this pathway affects AP progression and inflammatory cell activation. Furthermore, our research will extend to identifying and validating targeted inhibitors of this axis, with the ultimate goal of developing effective therapeutic interventions. These investigations will

provide crucial insights into the pathophysiological role of TNFα/TNFR1 axis in AP and establish novel diagnostic and therapeutic paradigms for clinical management.

Materials and Methods

AP patients

This study utilized human blood samples collected from the Department of Gastroenterology, The First Affiliated Hospital of Nanchang University. Blood was obtained from 69 patients, admitted within three days of their first episode of pancreatitis, and 8 healthy donors. Serum was separated by centrifugation at 4°C and stored for subsequent experiments.

Experimental animals

The study protocol involving animal experimentation received formal approval from the Institutional Animal Care and Use Committee of The First Affiliated Hospital of Nanchang University (proval number CDYFY-IACUC-202302QR076), complying with institutional, national and international animal welfare guidelines. Male C57BL/6 mice and Tnfrsf1a-/- mice were purchased from GemPharmatech Co., Ltd. (Nanjing, China) at 6 weeks of age.

Throughout the study period, all animals were maintained under SPF conditions and housed at 23 ± 2 °C under a 12-h light/dark cycle with free access to food and water ad libitum throughout experiments.

Experimental AP models

Three established AP models were included. Cerulein-induced AP model: Mice received 10 intraperitoneal (i.p.) injections of cerulein (100μg/kg/h; Sigma-Aldrich, Cat#C9026) at hourly intervals. Animals were euthanized at 24h post-first injection. L-Arginine Model: Mice received three i.p. injections of L-arginine–HCl (3 g/kg; Sigma-Aldrich, Cat#A5006) at hourly intervals. Necropsy was performed at 72h. Control groups received equivalent volumes of sterile phosphate-buffered saline (PBS) via identical routes and schedules. LIG model: Mice were anesthetized using a dedicated animal anesthesia system, secured under an anesthetic mask, and subjected to a 1 cm right upper abdominal incision; the pancreaticobiliary duct was then ligated near the duodenum with non-absorbable surgical sutures, followed by wound closure and disinfection. At 48h post-surgery, these mice received a single intraperitoneal injection of cerulein (50μg/kg) and were sacrificed at 72h. Sham-operated mice underwent identical procedures excluding duct ligation. Upon sacrifice, blood and pancreatic tissue samples were collected from all mice for further research.

Drug administration

To preemptively inhibit the TNFα–TNFR1 signaling axis in mice, intraperitoneal injections of specific inhibitors were administered once daily in the afternoon for 3 consecutive days prior to AP induction. For therapeutic intervention studies, inhibitors were delivered via intraperitoneal injection at 3h and 12h after

AP model initiation. Three pharmacological agents were used: Pomalidomide (Selleck, USA, Cat#S1567), Neurostatin-1 (Selleck, USA, Cat#S8037), and Infliximab (Selleck, USA, Cat#A2019) stock and working solutions were prepared according to the manufacturer's protocols.

H&E Staining and Scoring

The mice were euthanized 24h after AP modeling, and fresh pancreatic tissue was retrieved. The pancreatic tissues were fixed in 4% formalin for 24h, followed by embedding in paraffin and sectioning into 4μm slices for H&E staining. Histopathological features assessed included acinar edema, leukocyte infiltration, and (peri)pancreatic necrosis. Sections were evaluated and histological severity was scored following established criteria [22].

Immunohistochemistry and immunofluorescence

The immunohistochemistry (IHC) staining protocol involved sequential steps beginning with slide baking (60°C, 1h), xylene dewaxing (2×10min), and graded ethanol rehydration (100%→100%→95%→85%) followed by antigen retrieval in citrate (pH6.0) or EDTA (pH9.0, ZSGB-BIO, China) buffer using microwave heating (95°C,15min) and 30min cooling. Endogenous peroxidase was blocked with 3% H_2O_2 (8min, room temperature) before nonspecific binding blockade with 5% bovine serum albumin (BSA, Sigma-Aldrich, USA) (1h, room temperature). Primary antibodies (optimized dilution) were incubated overnight at 4°C. The following day, the samples were allowed to equilibrate at room temperature for 30 minutes before incubation with the IHC secondary antibody in a 37°C incubator (30 minutes). Signal development employed DAB substrate with hematoxylin counterstaining (10-30sec) and ammonia water bluing. Slides underwent graded ethanol dehydration (85%→95%→100%→100%), xylene clearing(2×10min), and DAPI mounting before bright-field microscopy and quantitative analysis using ImageJ software (V1.8.0) for threshold-based signal measurement.

The immunofluorescence (IF) protocol follows similar initial steps to standard IHC on day 1, including tissue processing, antigen retrieval, and blocking. The key modifications occur during antibody incubation: primary antibodies are applied at 4°C overnight (14-16 hours), followed on day 2 by incubation with species-matched fluorophore-conjugated secondary antibodies (1 hour at room temperature). After thorough washing, nuclei are counterstained with DAPI (Sigma-Aldrich, USA) prior to mounting. Fluorescent signals are then visualized and captured using confocal microscopy, with careful optimization of acquisition parameters to ensure specific signal detection while minimizing background and cross-channel bleed-through.

Quantitative reverse transcription polymerase chain reaction (qRT-PCR) analysis

Total RNA isolation: Pancreatic tissues from mice were homogenized, and total RNA was extracted using TRIzol™ Reagent (Invitrogen, Cat# 15596026CN) following manufacturer instructions. RNA quantification: RNA purity (A260/A280 ≥ 1.8) and concentration were measured using NanoDrop™ One Spectrophotometer (Thermo Fisher, v2.12.0). cDNA synthesis: First-strand cDNA was synthesized from 1

μg total RNA using the PrimeScript™ RT Reagent Kit with gDNA Eraser (TIANGEN, Cat# KR116) with random hexamer primers. Primer design: All qPCR primer pairs (including Gapdh control) were designed using Primer-BLAST and synthesized by Sangon Biotech (Shanghai). Annealing temperature: 60°C. Quantitative PCR: Reactions contained 2μL cDNA, 0.5μM forward/reverse primers, and 10μL Master Mix (YESAN, Cat# 11184ES08), 2μL cDNA, 0.8 μL each gene-specific primer (10 μM) in a 20 μL reaction volume. Relative gene expression was calculated via the 2−ΔΔCt method, normalized to Gapdh. The complete sequences of all primers utilized throughout this study are systematically documented in Supplementary Table S2.

Western blot analysis

The pancreatic protein was extracted using radio immunoprecipitation assay lysis buffer (Yesan, China) according to the manufacturer's protocol. Before western blot, the protein concentration was quantified using the bicinchoninic acid assay protein assay. Equal amounts of proteins were separated by sodium dodecyl sulfate - polyacrylamide gel electrophoresis and transferred to polyvinylidene fluoride membranes. After blocking with 5% skim milk, the membrane was probed with primary antibodies. After incubation with secondary antibodies for 1h at room temperature, bands were visualized using the Image-Lab (V6.0.1). The primary antibodies were diluted at 1:1000 in blocking buffer (5% BSA in tris-borate-sodium with Tween-20) for Western blot. The complete antibody information, including clone numbers, host species, dilution ratios, and commercial sources, is comprehensively documented in Supplementary Table S1 to ensure full experimental reproducibility.

ELISA detection

ELISA kits were obtained from Elabscience Biotechnology Co., Ltd. (Wuhan, China), and all assays were performed strictly according to the manufacturer's protocols. The following specific kits were used for cytokine quantification: TNFα (Catalog No. E-EL-M3063), IL-1β (Catalog No. E-EL-M0037), and IL-6 (Catalog No. E-EL-M0044). All assays included technical duplicates and were repeated in three independent experiments.

Bulk-RNA sequencing and data analysis

otal RNA was extracted from pancreatic tissues using TRIzol reagent, followed by quality assessment (RIN > 7.0, Agilent Bioanalyzer). Ribosomal RNA (rRNA) removed via NEBNext rRNA Depletion Kit, and libraries were prepared with the NEBNext Ultra II RNA Library Prep Kit. Paired-end sequencing (150 bp) was performed on an Illumina NovaSeq 6000 platform (~40 million reads/sample). Raw reads were quality-trimmed (Fastp, v0.23.2) and aligned to the mouse reference genome (GRCm38) using STAR (v2.7.8a). Gene-level counts were generated with featureCounts and normalized for differential expression analysis (DESeq2, v3.11, FDR < 0.05). Pathway enrichment was performed using KEGG and GO databases. All differential genes were listed in Supplementary Table S3.

Processing of Single-cell RNA sequencing (scRNA-seq)

Raw sequencing reads were stored in FASTQ format. Raw sequencing data underwent quality control to remove low-quality reads impacting downstream analyses.

Quality control. We processed the raw data using the open-source software fastp (v. 0.23.4) to obtain clean data for subsequent analysis. The filtering procedure included three main steps: 1) trimming 28 base pairs from read1; 2) retaining read2 sequences with average quality scores above 10; 3) removing read2 sequences containing 5 bases exceeding a specified threshold. The parameters used were "-w8 -l28 -n5 -q10 -b28 -B0".

Alignment & quantification. The initial processing of raw data employs CellRanger (v 7.1.0), which executes four key analytical steps: 1) correcting errors in cellular barcodes overlapped with known whitelists; 2) performing sequence alignment to a mm9 using the STAR (v2.7.8a); 3) conducting unique molecular identifier (UMI) correction and removing duplicates; 4) generating final gene expression profiles. Following this pipeline, a gene expression matrix was generated being suitable for subsequent quality filtering and in-depth analysis.

Cell Quality Control: We employed the Seurat (v4.3.0) under two criteria: 1) retaining cells with $200 \leq$ nFeature_RNA $\leq 6{,}000$; excluding cells with mitochondrial gene percentage > 20%.

Normalization, Reduction & Clustering. Technical noise was modeled using regularized negative binomial regression via SCTransform in Seurat. Principal Component Analysis (PCA) on highly variable genes (HVGs) were performed. The top N PCs were used for Uniform Manifold Approximation and Projection (UMAP). Cells were clustered via a K-nearest neighbor (KNN) graph, refined using Shared Nearest Neighbor (SNN), and partitioned using the Louvain algorithm.

Cell annotation: Clusters were annotated using SingleR (v2.0.0) with reference dataset X (Cite dataset).

Differential expression: Cluster marker genes were identified using FindAllMarkers (Seurat) with Wilcoxon Rank Sum test under following parameters: 1) genes expressed in ≥ 25% of cells in either cluster; 2) Bonferroni-adjusted p-value < 0.05; 3) Absolute log2(Fold Change) > 0.5

Functional enrichment: Statistically enriched GO terms, KEGG pathways[23], and Reactome pathways[24] among marker genes were identified using clusterProfiler (v4.16.0) with a threshold of adjusted p-value < 0.05.

Public sequencing data acquisition and processing

Publicly available scRNA-seq data (GSE188819; n=7 samples) were acquired from NCBI's Gene Expression Omnibus (GEO). The raw (or processed) count matrix was downloaded and processed using the Seurat (v4.3.0) toolkit in R. Specifically, cells with fewer than 200 genes or more than 20% mitochondrial reads were filtered out. Data normalization was performed using the LogNormalize method. The top 2000 highly variable genes were identified for downstream analysis.

Statistics

Quantitative data are reported as mean ± standard error of the mean (SEM). Statistical evaluations were carried out using GraphPad Prism (V7.0). For comparison of two experimental groups, either parametric Student's t-test or nonparametric Mann-Whitney U test was applied as appropriate based on data distribution characteristics. Multigroup analyses employed one-way ANOVA with Fisher's least significant difference post hoc testing. Bivariate correlations between microbial and metabolic variables were examined using Spearman's rank-order correlation coefficient. Histopathological assessments were conducted independently by two board-certified pathologists under blinded conditions. The threshold for statistical significance was established at $P < 0.05$ (two-tailed).

Results

The TNFα/TNFR1 axis is hyperactivated in murine models and patients with AP

As a pivotal inflammatory mediator in AP, TNFα signals through two distinct receptors, TNFR1(encoded by *Tnfrsf1a*) and TNFR2 (encoded by *Tnfrsf1b*). Analysis of ScRNA-seq dataset GSE188819 from an experimental AP model induced by caerulein revealed that *Tnf* was predominantly expressed in immune cells. In contrast, its receptor *Tnfrsf1a* was widely expressed across multiple pancreatic cell types, whereas *Tnfrsf1b* was expressed at low levels throughout pancreatic tissues (Fig. 1A). Cell-cell communication analysis further indicated that the TNF signaling network- primarily mediated by the TNFα/TNFR1 axis-was highly activated in AP (Fig. 1B). To investigate the expression of TNFα and TNFR1 in AP, we established three experimental AP models: caerulein-induced AP (CAE_AP), pancreatic duct ligation-induced AP (LIG_AP), and L-arginine-induced AP (ARG_AP) model. All models successfully constructed based on histopathological features such as pancreatic edema, inflammatory cell infiltration, and partial acinar cell necrosis, as shown by H&E staining (Fig. 1C, Fig. S1A, and S1B). Consistent with human AP manifestations, the CAE_AP model exhibited significant increases in serum lipase and amylase levels (Fig. 1D). Substantial inflammatory infiltration was further confirmed by IHC staining, with elevated expression of the macrophage marker F4/80 and neutrophil marker MPO (Fig. 1E, Fig S1C, and S1D). Similarly, mice with AP showed markedly higher serum levels of pro-inflammatory cytokines TNFα, IL-1β, and IL-6 compared to controls (Fig. 1F). Notably, we observed increased expression of TNFα and TNFR1 in all three experimental AP models relative to control mice (Fig. 1G-I). These observations were corroborated by Western blot analysis (Fig.1J). Furthermore, qRT-PCR analysis indicated upregulation of *Tnfα* and *Tnfr1* mRNA in AP mice (Fig. 1K).

Analysis of clinical serum samples showed significantly elevated TNFα levels in AP patients compared to healthy controls, with levels increasing in accordance with disease severity (Fig. 1L). Although not statistically significant overall, TNFR1 was elevated in severe AP (SAP) cases (Fig. 1M). Taken together, these results confirmed activation of the TNFα/TNFR1 signaling axis in human and mouse AP.

Genetic TNFR1 ablation ameliorates inflammatory response in AP

To investigate the role of the TNFα/TNFR1 axis in the pathogenesis of AP, we generated conventional global *Tnfr1* knockout (*Tnfr1*$^{-/-}$) mice. Successful ablation of *Tnfr1* was confirmed by genotyping and qRT-PCR analysis (Fig. S2A and S2B). Then, AP were induced in both WT and *Tnfr1*$^{-/-}$ mice using two established models: caerulein injections and pancreatic duct ligation. Histopathological analysis indicated a significant reduction in pancreatic inflammation in *Tnfr1* deficient mice than in WT controls following the induction of AP via CAE injection or PDL (Fig. 2A-B). Consistently, the neutrophil marker MPO and macrophage marker F4/80 was markedly reduced in the pancreatic tissues of *Tnfr1*$^{-/-}$ mice with AP compared to WT controls (Fig. 2A, 2C and 2D). Further supporting this notion, qRT-PCR analysis of pancreatic tissue revealed a significant downregulation of pro-inflammatory cytokines, including *Tnfα*, *Il1b*, and *Il6*, in both CAE- and PDL-induced AP models of *Tnfr1*$^{-/-}$ mice compared to WT group (Fig. 2E). We next assessed the NF-κB and STAT3 pathways, which are activated by TNF/TNFR1 signaling and play well-established role in proinflammatory response. Phosphorylation of P65 and STAT3 was markedly elevated in CAE_AP WT mice, whereas this effect was abolished in *Tnfr1* deficient mice with AP (Fig. 2F and S2D). However, serum amylase and lipase levels remained comparable between genotypes (Fig. S2C). Furthermore, immunofluorescence staining for the markers CITH3 and MPO was performed to assess the neutrophil extracellular traps (NETs) formation. Notably, there was a pronounced reduction in CITH3+MPO+ NETs structures in the pancreatic tissues of *Tnfr1*$^{-/-}$ mice with AP relative to their WT counterparts (Fig. 2G). In agreement with this data, serum cfDNA levels were also significantly decreased in *Tnfr1*$^{-/-}$ AP mice (Fig. 2H). Collectively, these data revealed that *Tnfr1* deficiency significantly attenuates inflammatory infiltration during AP progression.

Single-cell analysis uncovers altered immune landscape in TNFR1-depleted AP mice

To define the comprehensive cellular mechanisms by which *Tnfr1* deficiency modulates inflammatory responses, we conducted scRNA-seq to compare the cellular heterogenicity and phenotype-specific alterations across various cell populations between WT and *Tnfr1*$^{-/-}$ mice with CAE-induced AP (Fig. 3A). Unsupervised clustering of transcriptomes identified eight major cell populations (Fig. 3B), annotated based on specific cell markers: Myeloid cells (*Lyz2*, *S100a4*, *C1qb*), Neutrophils (*S100a8*, *S100a9*, *G0s2*), Fibroblasts (*Col1a1*, *Dcn*, *Pdgfra*), Acinar cells (*Ctrb1*, *Try5*, *Prss2*, *Cpb1*), B cells (*Cd79a*, *Igkc*, *Ighm*), Endothelial cells (*Pecam1*, *Plvap*), T cells (*Cd3d*, *Cd3e*) and Ductal cells (*Krt8*, *Krt18*) (Fig. 3C). Cell-type identity was further validated by distinct gene expression patterns in a heatmap (Fig. S3A).

Comparative analysis revealed a marked reduction in myeloid and neutrophil populations in *Tnfr1*$^{-/-}$ mice, along with an expansion of the acinar cell compartment (Fig. 3E, 3F), consistent with our previous observations of attenuated inflammation. Flow cytometry confirmed decreased infiltration of neutrophils ($CD11b^{+}Ly6G^{+}$) and macrophages ($CD11b^{+}F4/80^{+}$) in *Tnfr1*$^{-/-}$ mice with AP compared to the WT AP group (Fig. 3G). In agreement with scRNA-seq findings, immunofluorescence staining showed a significant increase in the acinar marker Amylase, alongside reduced expression of the myeloid marker LYZ and the neutrophil marker S100A9, in pancreatic tissues of *Tnfr1*-deficient AP mice relative to WT controls (Fig.

3H and I). These results align with earlier data demonstrating that Tnfr1 knockout leads to a substantial decrease in immune cells infiltration in AP models.

Multi-omics integration reveals that *Tnfr1* ablation impairs neutrophil and macrophage recruitment and inflammatory cytokine release

we conducted bulk RNA sequencing on pancreatic tissues from both WT and *Tnfr1*$^{-/-}$ mice to establish a comprehensive transcriptional landscape. This integrated multi-omics approach enabled more precise identification of inflammation-associated key genes through cross-platform validation. Principal component analysis of the bulk transcriptome data revealed high intra-group reproducibility and substantial inter-group separation (Fig. 4A). Volcano plot analysis identified numerous significantly differentially expressed genes (DEGs), with heatmaps displaying genes upregulated or downregulated in *Tnfr1*$^{-/-}$ mice (Fig. 4C, D).

Cross-referencing these DEGs with scRNA-seq data, we identified 11 genes (*Ifi209*, *Gpr65*, *Phf11b*, *Marcksl1*, *Cxcr4*, *Ifit3*, *Treml2*, *Oas3*, *Rab44*, *Bhlha15*, and *Acvr1c*) showing consistent expression trends across both sequencing platforms (Fig. 4E). Among the *Tnfr1*-dependent genes identified, a substantial proportion were functionally linked to type I interferon signaling (IFN), suggesting that the TNFα/TNFR1 axis exacerbates AP inflammation, at least in part, by potentiating IFN production and downstream inflammatory responses. Functional annotation revealed that upregulated genes in WT group were enriched in inflammatory and immune responses. However, *Bhlha15* and *Acvr1c* were upregulated in acinar cells from *Tnfr1*$^{-/-}$ group, may contribute to acinar cell homeostasis. Cell-type-specific mapping revealed that WT-upregulated genes localized predominantly to myeloid cells (*Ifi209*, *Gpr65*, *Phf11b*) and neutrophils (*Marcksl1*, *Cxcr4*, *Ifit3*, *Treml2*, *Oas3*, *Rab44*), whereas upregulated genes (*Bhlha15*, *Acvr1c*) were specific to acinar cells from *Tnfr1*$^{-/-}$ group.

qRT-PCR validation confirmed most pro-inflammatory DEGs (except *Phf11b* and *Treml2*), while acinar cell-associated genes showed inconsistent trends: *Acvr1c*: non-significant increase, *Bhlha15*: opposite trend (Fig. 4F). Notably, inflammation-related genes exhibited robust concordance in both sequencing, underscoring the reliability of our multi-omics approach in identifying TNFR1-regulated inflammatory mediators.

Neutrophils in *Tnfr1*$^{-/-}$ mice exhibit loss of *Marcksl1*, *Ifit3*, and *Oas3* with emergence of an inflammatory suppression subcluster

Following confirmation of significant inflammatory cell alterations upon *Tnfr1* ablation, we performed neutrophil-specific transcriptional profiling through dimensionality reduction and clustering, identifying six transcriptionally distinct subclusters (Fig. 5A). Comparative UMAP visualization revealed differential distribution between two groups, with near-exclusive derivation of the Neu_3 subclusters from *Tnfr1*$^{-/-}$ mice (Fig. 5B), which was straightly show in the proportional bar chart (Fig. 5C). Heatmap analysis of subpopulation-specific top 10 marker genes revealed different transcriptional signatures predictive of functional heterogeneity (Fig. 5D). Neu_1 and Neu_4 were predominant subsets in WT mice, with

functional analysis indicating Neu_1 involvement in primary immune response activation and Neu_4 enrichment in chemokine/TNF signaling pathways (Fig. 5E). Conversely, *Tnfr1*$^{-/-}$ mice exhibited Neu_3 subcluster predominance characterized by inflammatory suppression properties (Fig. 5F), mechanistically explaining their attenuated inflammatory phenotype. Consistent with the observed reduction in NETs release in *Tnfr1*$^{-/-}$ mice, gene set enrichment analysis (GSEA) revealed significant downregulation of NETosis-related pathways compared to WT group. Expression profiling localized NET-associated genes predominantly to pro-inflammatory Neu_1/Neu_4 subclusters (Fig. 5G). The neutrophil-specific genes (*Marcksl1*, *Cxcr4*, *Ifit3*, *Treml2*, *Oas3*, *Rab44*) demonstrating specific upregulation in WT group, with single-cell resolution confirming predominant Neu_1 expression (Fig. 5H). Three key mediators were characterized: *Ifit3* potentiates interferon-driven cytokine production; *Marcksl1* regulates cytoskeletal dynamics essential for ROS generation and NETosis; *Oas3* mediates type I interferon-induced pro-inflammatory signaling. Elevated MARCKSL1 protein expression in WT neutrophils was confirmed by IHC staining. Collectively, WT neutrophils exhibit pro-inflammatory activation states whereas *Tnfr1* deficiency promotes an inflammatory suppressionNeu_3 cluster that fundamentally attenuates inflammatory responses.

The unique Myeloid_Igkc subcluster in *Tnfr1*$^{-/-}$ mice suppresses inflammatory responses in AP

Given the emergence of unique neutrophil subpopulations following *Tnfr1* deletion, we next investigated whether similarly distinct alterations occur in other inflammation-associated myeloid cells. Re-clustering analysis of myeloid cells based on highly expressed markers identified five principal subsets: macrophages (*C1qa*, *C1qb*), monocytes (*Ly6c*), dendritic cells (*Cd209a*, *Flt3*), and two novel myeloid subsets (Fig. 6A, s5A). Further subclustering of macrophages revealed four transcriptionally distinct subclusters (Fig. 6B).

Comparative analysis revealed striking distribution differences: the Myeloid_Igkc was almost exclusively derived from *Tnfr1*$^{-/-}$ mice, while Macro_C3 and Monocytes predominated in WT group (Fig. 6C). The result of M1 score showed that *Tnfr1*$^{-/-}$ mice get lower M1 score, which means less proinflammation myeloid cell (Fig. 6D). The KEGG pathway enrichment analysis revealed significant upregulation of TNFα signaling and chemokine pathways in Macro_C3, and Monocytes led to the formation of neutrophil extracellular trap, contrasting with marked downregulation in Myeloid_Igkc (Fig. 6E). These findings parallel our neutrophil observations, demonstrating that *Tnfr1* deletion similarly reprograms myeloid cell functionality to attenuate inflammatory responses. To investigate the communication activity of two specific cell subpopulations (Neu_c3 and Myeloid_Igkc), we performed cell communication analysis focusing on acinar cells, neutrophils, and myeloid cells (Fig. 6F). The results revealed that Neu_c3 exhibits minimal communication activity, potentially attributable to the expression of inflammatory suppression genes which may dampen its own activation. In contrast, Myeloid_Igkc demonstrates highly active communication, suggesting that its inflammatory suppression function may be exerted through interactions with other cells to mitigate inflammatory responses. In one word, these results underscore the pivotal role of the TNFα/TNFR1 axis in driving inflammatory progression during AP.

Prophylactic blockade of TNFα/TNFR1 axis by pomalidomide ameliorates inflammation and acinar cell damage in AP

Our previous findings revealed that TNFα promotes inflammatory progression in AP through TNFR1 binding, and that *Tnfr1* knockout alleviated AP inflammation. To bridge these findings with clinical therapeutic potential, we investigated three distinct inhibitors of the TNFα/TNFR1 axis: infliximab, necrostatin-1, and pomalidomide. Drugs were administered daily for 3 days prior to AP induction to establish TNFα/TNFR1 axis inhibition before disease modeling (Fig. 7A). Among the three inhibitors, pomalidomide showed the most significant ameliorative effects on AP, as evidenced by reduced acinar cell necrosis and diminished inflammatory responses (Fig. 7B, 7C). The optimal dosage of pomalidomide was determined to be 0.5 mg/kg (hereafter referred to as the Pom group). And then, we found that, compared with vehicle group, serum amylase and lipase levels were significantly reduced in the Pom group (Fig. 7D). IHC staining revealed decreased neutrophil and macrophage infiltration in Pom-treated mice, accompanied by downregulation of inflammatory cytokines (*TNFα*, *Il1b*, and *Il6*) as measured by qRT-PCR analysis (Fig. 7E, F). Concurrently, NETs release was also reduced in the Pom group (Fig. 7H). These results collectively demonstrate that pomalidomide alleviates AP inflammation through inhibition of the TNFα/TNFR1 axis. To further examine whether pom-mediated AP improvement mirrors the effects observed in *Tnfr1*$^{-/-}$ mice, we validated previously identified differentially expressed genes from single-cell RNA sequencing and bulk transcriptome analyses. Remarkably, qRT-PCR results of these genes showed consistent expression patterns with prior findings (Fig. 7G). These data not only confirmed that pomalidomide specifically inhibits the TNFα/TNFR1 axis, but also established a solid preclinical foundation for future clinical applications.

Intraperitoneal pomalidomide administration after AP induction still shows therapeutic effects in mice

Building upon our previous findings demonstrating that preemptive inhibition of the TNFα/TNFR1 axis effectively mitigates AP severity, we next investigated the therapeutic potential of post-onset intervention. We established a modified treatment protocol involving intraperitoneal administration of pomalidomide at 3- and 12-hours following AP induction (Fig 8A). Consistent with our prophylactic findings, therapeutic administration of pomalidomide at 0.5 mg/kg revealed robust efficacy in ameliorating AP severity (Fig. 8B). Comprehensive analysis revealed Pom significantly attenuated pancreatic inflammation, evidenced by histopathological improvement (Fig. 8C) and reduced IHC staining of MPO and F4/80 (Fig. 8D). Moreover, qRT-PCR analysis confirmed marked downregulation of key inflammatory factors (*TNFα*, *Il-6*, *Il-1β*) in pancreatic tissue (Fig. 8E), accompanied by reduced serum amylase and lipase levels (Fig. 8F). Notably, pomalidomide treatment significantly impaired NETs formation (Fig. 8G). Furthermore, to confirm the absence of organ toxicity induced by pomalidomide in this experiment, H&E staining was performed on various organs as supporting evidence (Fig. 8H). These results conclusively demonstrate that pharmacological inhibition of the TNFα/TNFR1 axis effectively treats established AP in murine models, warranting further investigation of its clinical potential for human AP management.

Discussion

The TNFα/TNFR1 axis plays a pivotal role in inflammatory diseases, yet its function in AP pathogenesis remains poorly understood. Our study bridges this critical knowledge gap. We first revealed the consistent upregulation of the TNFα/TNFR1 axis across three distinct AP animal models. To elucidate its mechanistic contributions, we generated *Tnfr1*$^{-/-}$ mice and induced AP. Strikingly, disruption of TNFα/TNFR1 axis markedly attenuated pancreatic inflammation. Leveraging scRNA-seq of pancreatic tissues from *Tnfr1*$^{-/-}$ and WT mice after CAE_AP modeling, we uncovered a significant reduction in neutrophil and myeloid cell infiltration—validated by flow cytometry and IF staining. Subcluster analysis revealed, for the first time, the emergence of inflammatory suppression myeloid and neutrophil subsets in *Tnfr1*$^{-/-}$ mice. Integrated bulk RNA-seq further identified *Tnfr1* deletion-dependent genes specifically enriched in neutrophils (*Marcksl1*, *Cxcr4*, *Ifit3*, *Treml2*, *Oas3*, *Rab44*) and myeloid cells (*Ifi209*, *Gpr65*, *Phf11b*). These genes, downregulated upon *Tnfr1* ablation, may represent key molecular effectors of TNFα/TNFR1-driven inflammation. To therapeutically target this signaling, we employed pomalidomide, a clinically relevant inhibitor. Notably, intraperitoneal administration of pomalidomide—either pre- or post-AP induction—dramatically ameliorated disease severity, suppressing inflammation and reducing acinar cell necrosis. Our findings not only provide a robust experimental foundation for AP treatment but also unveil a druggable target, offering transformative clinical potential.

The TNFα/TNFR1 axis has been consistently implicated in mediating inflammatory responses and apoptotic processes across multiple disease states. Emerging evidence demonstrates that TNFα/TNFR1 axis is essential for both acute and chronic itch through peripheral and central mechanisms, with Tnfr1 knockout mice exhibiting attenuated scratching behaviors - suggesting therapeutic potential for chronic pruritus[25]. Notably, Tnfr1 deficiency reduces keratinocyte apoptosis and inflammatory cytokine release without compromising epidermal differentiation, positioning this pathway as a promising target for dermatological disorders[26]. Beyond cutaneous pathologies, *Tnfr1* ablation impedes melanoma progression by modulating tumor cell proliferation, migration, angiogenesis, and CD8+ T cell recruitment/activation, highlighting how disrupting TNFα/TNFR1 axis may control neoplastic growth[27]. These collective findings establish the TNFα/TNFR1 axis as a master regulator of tissue inflammation and apoptotic cascades, where pathway inhibition consistently ameliorates disease pathogenesis - a conclusion strongly supported by our experimental results.

scRNA-seq surpasses conventional bulk transcriptomics in resolution, enabling deep profiling at the individual cell level and revolutionizing research across disciplines[28, 29]. This powerful technology reveals disease-associated shifts in cellular composition, transcriptional heterogeneity, and previously unrecognized cell subsets. Neutrophils, as the first responders in acute inflammation[30, 31], exhibited remarkable reprogramming in *Tnfr1*$^{-/-}$ mice, where we identified a novel neutrophil subpopulation (Neu_3) with distinct inflammatory suppression properties. GSEA analysis revealed that Neu_3 cells differentially expressed immunoregulatory genes (*Entpd3*, *Ptgs1*, *Mrps24*, *Igfbp6*) compared to conventional neutrophils. Notably, *Entpd3* encodes a membrane-bound glycoprotein that modulates purinergic

signaling through extracellular ATP/ADP hydrolysis, with elevated expression conferring protection against intestinal inflammation in Crohn's disease[32]. Similarly, *Ptgs1* mediates anti-inflammatory eicosanoid production, consistent with the known gastrointestinal benefits of COX-2 inhibitors[33]. These findings indicate that *Tnfr1* deletion attenuates pro-inflammatory neutrophil activation while enhancing their immunoregulatory capacity. Mirroring this phenomenon, *Tnfr1*$^{-/-}$ mice uniquely developed an inflammatory suppression myeloid subset (Myeloid_Igkc), collectively demonstrating how *Tnfr1* ablation reprograms inflammatory cells toward an anti-inflammatory phenotype, thereby mitigating pancreatic inflammation in AP.

Integrative analysis of scRNA-seq and bulk RNA sequencing revealed significant upregulation of *Ifi209*, *Gpr65*, *Phf11b*, *Marcksl1*, *Cxcr4*, *Ifit3*, *Treml2*, *Oas3*, and *Rab44* in WT mice, with these genes predominantly expressed in neutrophils and myeloid cells - the key inflammatory cell populations. Notably, *Ifi209*, *IFIT3*, and *OAS3* directly regulate interferon signaling[34, 35], while *Treml2*, *Cxcr4* and *Gpr65* modulate interferon responses indirectly[36-38]. Although current literature predominantly positions the TNFα/TNFR1 axis signaling as operating in parallel with interferon pathways to coordinately regulate immune responses and apoptosis[39], our findings suggest a novel hierarchical relationship in acute pancreatitis, where the TNFα/TNFR1 axis may actually drive disease progression by promoting interferon synthesis and release.

In our search for effective inhibitors of the TNFα/TNFR1 axis, we systematically evaluated three distinct compounds: infliximab, necrostatin-1, and pomalidomide. Infliximab, a clinically established TNFα-neutralizing antibody, has revealed efficacy in treating inflammatory bowel disease and autoimmune hepatitis[40, 41], though its organ toxicity remains a significant clinical concern[42]. Necrostatin-1, while not directly interfering with TNFα/TNFR1 axis per se, acts downstream by inhibiting receptor-interacting protein kinase 1 to block TNFα-induced necroptosis[43] . Pomalidomide, a clinically approved chemotherapeutic agent typically combined with dexamethasone for multiple myeloma treatment[44, 45], operates through a unique mechanism by enhancing mRNA degradation enzymes (e.g., Ikaros/Aiolos) to suppress TNFα transcription and secretion. Our experimental data revealed pomalidomide as the most potent therapeutic candidate for AP. While immunosuppressants find broad clinical applications, their use in AP has been largely restricted to autoimmune pancreatitis (AIP), where oral corticosteroids remain the standard treatment and rituximab is reserved for recurrent AIP cases[46]. Our study not only identifies promising therapeutic targets for AP but also provides a robust experimental foundation for immunomodulatory intervention. However, rigorous monitoring of potential off-target organ toxicity through long-term clinical studies will be essential for translational application.

While this study presents significant novel findings, several limitations warrant discussion. First, we have not fully elucidated the molecular mechanisms of the TNFα/TNFR1 axis signaling, particularly regarding its upstream transcriptional regulators and downstream effectors. Second, although we identified differentially expressed genes in neutrophils and macrophages that likely interact with the TNFα/TNFR1 axis to modulate AP progression, these candidates remain to be functionally validated

through pharmacological interventions (inhibitors/activators) in AP models. Furthermore, our scRNA-seq analysis requires deeper exploration, particularly concerning acinar cell alterations and functional characterization of the newly identified immune cell subsets. These limitations directly inform our future research directions: we will systematically investigate the downstream molecular consequences of *Tnfr1* ablation, delineate its impact on acinar cell biology, and experimentally validate the candidate genes identified through multi-omics analysis to assess their effects on TNFα/TNFR1 axis and AP severity. Collectively, these efforts aim to establish a comprehensive TNFα/TNFR1-centric regulatory pathway governing pancreatic inflammation, potentially revealing novel therapeutic strategies for AP management.

Building upon the observed elevation of the TNFα/TNFR1 axis in AP, our multi-model study establishes its critical role in driving inflammatory responses, demonstrating that *Tnfr1* knockout significantly attenuates pancreatic inflammation in murine AP. Through integrated single-cell and bulk transcriptomic analyses, we uncovered a marked downregulation of interferon-related genes following *Tnfr1* ablation, accompanied by the emergence of unique inflammatory suppression neutrophil and myeloid cell subpopulations. Most notably, we identified pomalidomide as a potent therapeutic agent that not only ameliorates inflammation but also protects against acinar cell death. Our work systematically delineates the TNFα/TNFR1 axis as a master regulator of AP pathogenesis, revealing its dual impact on both gene expression programs and immune cell polarization. The discovery of pomalidomide's efficacy in AP management represents a conceptual advance, opening new therapeutic eyesight and suggesting promising immunomodulatory strategies for clinical translation.

Declarations

Data Availability

The transcriptomic and sequencing data discussed in this publication have been deposited in the GEO archive (GSE309230, GSE306650).

Grant support

We gratefully acknowledge the financial support from the Academic and Technical Leader of Major Disciplines in Jiangxi Province (20225BCJ23021) and the Natural Science Foundation of Jiangxi Province (20224ACB216004). This work was also supported by grants from the National Natural Science Foundation of China (82260133, 82370661) and the Technological Innovation Team Cultivation Project of the First Affiliated Hospital of Nanchang University (YFYKCTDPY202202).

Author contributions

Yin Zhu and Nianshuang Li conceived and designed the study, and supervised its progress. Xiaoli Xi was responsible for troubleshooting experimental issues. Pan Zheng and Xueyang Li performed the animal experiments and contributed to manuscript writing. Yuman Ye carried out the single-cell and

transcriptome data analysis, with assistance from Dongni Fu in data analysis. Maobin Kuang and Yaoyu Zou were responsible for mouse husbandry and participated in the animal experiments. Jianhua Wan and Cong He participated in data analysis and manuscript review. Nonghua Lv oversaw the manuscript review.

Acknowledgments

We thank Haplox biotech company (Shangrao, China) for the support of scRNA-seq analysis and Majorbio Bio-Pharm Technology Co.,Ltd (Shanghai, China) for the support of bulk RNA sequencing analysis. We gratefully acknowledge Jiangsu GemPharmatech Co., Ltd. For providing the wild-type and *Tnfr1*$^{-/-}$ mice used in this study.

Ethics approval and consent to participate

This work was approved by the Ethics Committee of the First Affiliated Hospital of Nanchang University under protocol number (2023) CDYFYYLK (08-011) and (2024) CDYFYYLK (06-039). All tissue samples were obtained under informed consent.

Conflict of interest

The authors declare that they have no competing interests.

References

1. Gardner TB. Acute Pancreatitis. Ann Intern Med 2021;174:ITC17-ITC32.
2. Mederos MA, Reber HA, Girgis MD. Acute Pancreatitis: A Review. JAMA 2021;325:382-390.
3. Lee PJ, Papachristou GI. New insights into acute pancreatitis. Nat Rev Gastroenterol Hepatol 2019;16:479-496.
4. Habtezion A, Gukovskaya AS, Pandol SJ. Acute Pancreatitis: A Multifaceted Set of Organelle and Cellular Interactions. Gastroenterology 2019;156:1941-1950.
5. Glaubitz J, Asgarbeik S, Lange R, et al. Immune response mechanisms in acute and chronic pancreatitis: strategies for therapeutic intervention. Front Immunol 2023;14:1279539.
6. Kalliolias GD, Ivashkiv LB. TNF biology, pathogenic mechanisms and emerging therapeutic strategies. Nat Rev Rheumatol 2016;12:49-62.
7. He S, Wang L, Miao L, et al. Receptor interacting protein kinase-3 determines cellular necrotic response to TNF-alpha. Cell 2009;137:1100-11.
8. Locksley RM, Killeen N, Lenardo MJ. The TNF and TNF receptor superfamilies: integrating mammalian biology. Cell 2001;104:487-501.
9. Siegmund D, Wajant H. TNF and TNF receptors as therapeutic targets for rheumatic diseases and beyond. Nat Rev Rheumatol 2023;19:576-591.

10. Probert L. TNF and its receptors in the CNS: The essential, the desirable and the deleterious effects. Neuroscience 2015;302:2-22.
11. Hayden MS, Ghosh S. Regulation of NF-kappaB by TNF family cytokines. Semin Immunol 2014;26:253-66.
12. Annibaldi A, Meier P. Checkpoints in TNF-Induced Cell Death: Implications in Inflammation and Cancer. Trends Mol Med 2018;24:49-65.
13. Liu L, Sandow JJ, Leslie Pedrioli DM, et al. Tankyrase-mediated ADP-ribosylation is a regulator of TNF-induced death. Sci Adv 2022;8:eabh2332.
14. van Loo G, Bertrand MJM. Death by TNF: a road to inflammation. Nat Rev Immunol 2023;23:289-303.
15. Preedy MK, White MRH, Tergaonkar V. Cellular heterogeneity in TNF/TNFR1 signalling: live cell imaging of cell fate decisions in single cells. Cell Death Dis 2024;15:202.
16. Fei X, Chen S, Li L, et al. Helicobacter pylori infection promotes M1 macrophage polarization and gastric inflammation by activation of NLRP3 inflammasome via TNF/TNFR1 axis. Cell Commun Signal 2025;23:6.
17. Kanwar M, Dey R, Maiti S, et al. Synovial macrophages of rheumatoid arthritic mice protectively responded by altered M1/M2 differentiation after antibody blocking of TNFR1 and IL-1R. Int Immunopharmacol 2023;115:109654.
18. Shibata H, Yoshioka Y, Abe Y, et al. The treatment of established murine collagen-induced arthritis with a TNFR1-selective antagonistic mutant TNF. Biomaterials 2009;30:6638-47.
19. Wang Z, Wang W, Xu J, et al. Development and validation of dynamic clinical subphenotypes in acute pancreatitis patients using vital sign trajectories in intensive care units: a multinational cohort study. Signal Transduct Target Ther 2025;10:180.
20. Kusske AM, Rongione AJ, Reber HA. Cytokines and acute pancreatitis. Gastroenterology 1996;110:639-42.
21. Staubli SM, Oertli D, Nebiker CA. Laboratory markers predicting severity of acute pancreatitis. Crit Rev Clin Lab Sci 2015;52:273-83.
22. Schmidt J, Rattner DW, Lewandrowski K, et al. A better model of acute pancreatitis for evaluating therapy. Ann Surg 1992;215:44-56.
23. Kanehisa M, Furumichi M, Sato Y, et al. KEGG: biological systems database as a model of the real world. Nucleic Acids Res 2025;53:D672-D677.
24. Fabregat A, Sidiropoulos K, Viteri G, et al. Reactome pathway analysis: a high-performance in-memory approach. BMC Bioinformatics 2017;18:142.
25. Miao X, Huang Y, Liu TT, et al. TNF-alpha/TNFR1 Signaling is Required for the Full Expression of Acute and Chronic Itch in Mice via Peripheral and Central Mechanisms. Neurosci Bull 2018;34:42-53.
26. Piao X, Miura R, Miyake S, et al. Blockade of TNF receptor superfamily 1 (TNFR1)-dependent and TNFR1-independent cell death is crucial for normal epidermal differentiation. J Allergy Clin Immunol

2019;143:213-228 e10.
27. Rodriguez YI, Campos LE, Castro MG, et al. Tumor Necrosis Factor Receptor-1 (p55) Deficiency Attenuates Tumor Growth and Intratumoral Angiogenesis and Stimulates CD8(+) T Cell Function in Melanoma. Cells 2020;9.
28. Van de Sande B, Lee JS, Mutasa-Gottgens E, et al. Applications of single-cell RNA sequencing in drug discovery and development. Nat Rev Drug Discov 2023;22:496-520.
29. Papalexi E, Satija R. Single-cell RNA sequencing to explore immune cell heterogeneity. Nat Rev Immunol 2018;18:35-45.
30. Liew PX, Kubes P. The Neutrophil's Role During Health and Disease. Physiol Rev 2019;99:1223-1248.
31. Shao S, Xue K, Wang G. Neutrophils in neutrophilic dermatoses: Emerging roles and promising targeted therapies. J Allergy Clin Immunol 2022;149:1203-1205.
32. Feldbrugge L, Moss AC, Yee EU, et al. Expression of Ecto-nucleoside Triphosphate Diphosphohydrolases-2 and -3 in the Enteric Nervous System Affects Inflammation in Experimental Colitis and Crohn's Disease. J Crohns Colitis 2017;11:1113-1123.
33. Bjarnason I, Scarpignato C, Holmgren E, et al. Mechanisms of Damage to the Gastrointestinal Tract From Nonsteroidal Anti-Inflammatory Drugs. Gastroenterology 2018;154:500-514.
34. Wu YY, Xing J, Li XF, et al. Roles of interferon induced protein with tetratricopeptide repeats (IFIT) family in autoimmune disease. Autoimmun Rev 2023;22:103453.
35. Choi UY, Kang JS, Hwang YS, et al. Oligoadenylate synthase-like (OASL) proteins: dual functions and associations with diseases. Exp Mol Med 2015;47:e144.
36. Hashiguchi M, Kobori H, Ritprajak P, et al. Triggering receptor expressed on myeloid cell-like transcript 2 (TLT-2) is a counter-receptor for B7-H3 and enhances T cell responses. Proc Natl Acad Sci U S A 2008;105:10495-500.
37. Arazi A, Rao DA, Berthier CC, et al. The immune cell landscape in kidneys of patients with lupus nephritis. Nat Immunol 2019;20:902-914.
38. Larabi A, Barnich N, Nguyen HTT. New insights into the interplay between autophagy, gut microbiota and inflammatory responses in IBD. Autophagy 2020;16:38-51.
39. Hoekstra ME, Slagter M, Urbanus J, et al. Distinct spatiotemporal dynamics of CD8(+) T cell-derived cytokines in the tumor microenvironment. Cancer Cell 2024;42:157-167 e9.
40. Choy MC, Li Wai Suen CFD, Con D, et al. Intensified versus standard dose infliximab induction therapy for steroid-refractory acute severe ulcerative colitis (PREDICT-UC): an open-label, multicentre, randomised controlled trial. Lancet Gastroenterol Hepatol 2024;9:981-996.
41. Efe C, Lytvyak E, Eskazan T, et al. Efficacy and safety of infliximab in patients with autoimmune hepatitis. Hepatology 2025;81:1660-1670.
42. Bjornsson HK, Gudbjornsson B, Bjornsson ES. Infliximab-induced liver injury: Clinical phenotypes, autoimmunity and the role of corticosteroid treatment. J Hepatol 2022;76:86-92.

43. Cao L, Mu W. Necrostatin-1 and necroptosis inhibition: Pathophysiology and therapeutic implications. Pharmacol Res 2021;163:105297.
44. Dimopoulos MA, Terpos E, Boccadoro M, et al. Daratumumab plus pomalidomide and dexamethasone versus pomalidomide and dexamethasone alone in previously treated multiple myeloma (APOLLO): an open-label, randomised, phase 3 trial. Lancet Oncol 2021;22:801-812.
45. Dimopoulos MA, Dytfeld D, Grosicki S, et al. Elotuzumab plus Pomalidomide and Dexamethasone for Multiple Myeloma. N Engl J Med 2018;379:1811-1822.
46. Nista EC, De Lucia SS, Manilla V, et al. Autoimmune Pancreatitis: From Pathogenesis to Treatment. Int J Mol Sci 2022;23.

Figures

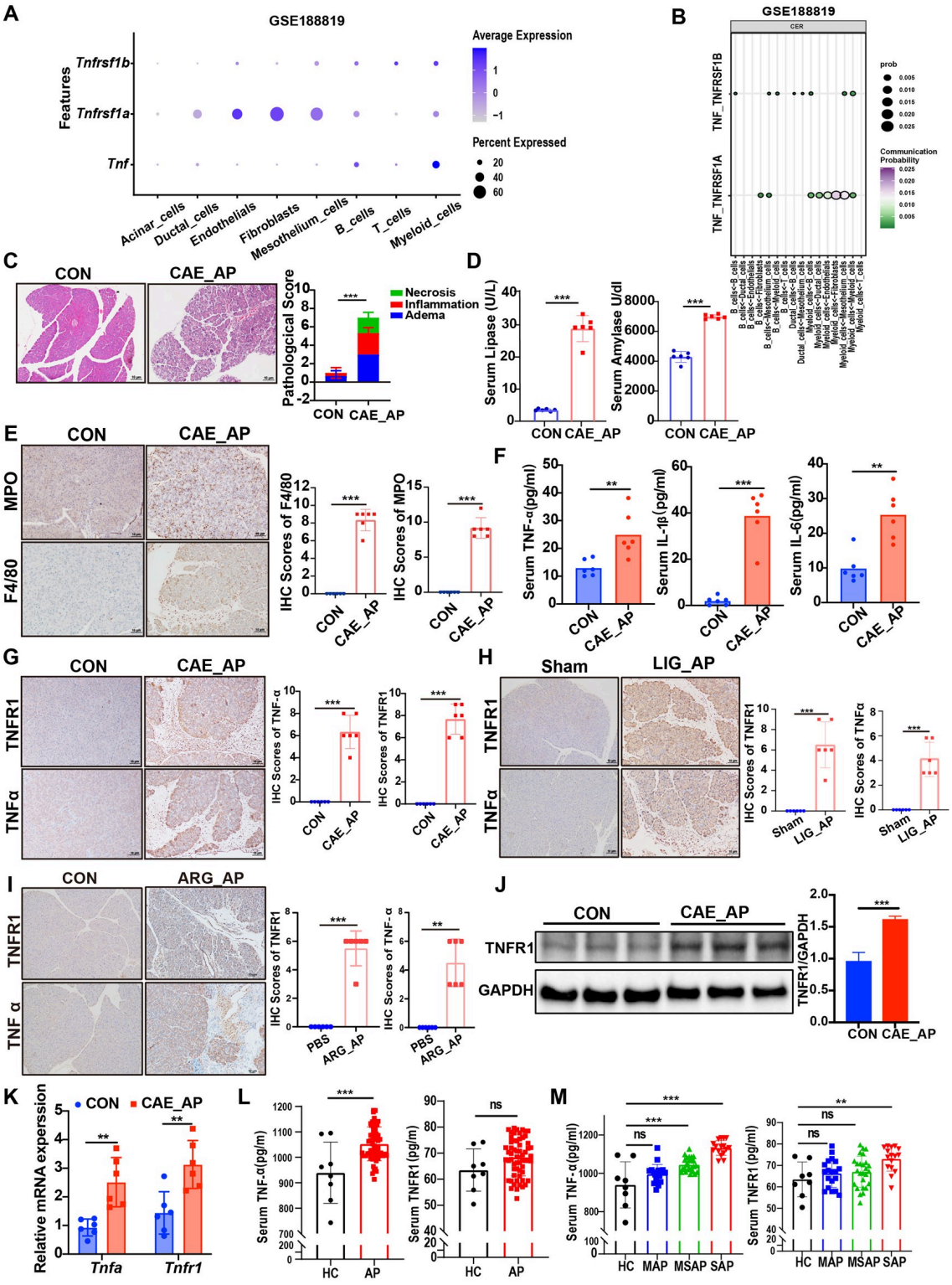


Figure 1

Activation of the TNFα/TNFR1 axis in three AP animal models. (A) Single cell RNA sequencing illustrating the expression of tumor necrosis factor-α *(Tnfa)*, tumor necrosis factor receptor superfamily member 1a *(Tnfrsf1a)*, and member 1b *(Tnfrsf1b)* genes across various cell types in CER induced AP.; (B) Cellular communication analysis suggests reveals enhanced ligand-receptor interaction probability between *Tnfa* and *Tnfrsf1b*. (C) Representative H&E-stained pancreatic tissue sections (scale bar: 10 μm)

and pathological scoring in control and cerulein-induced AP (CAE_AP) model mice. (D) Serum lipase and amylase levels in control and CAE_AP mice. (E) Immunohistochemical (IHC）assessment of neutrophil infiltration (myeloperoxidase, MPO) and macrophage accumulation (F4/80) in pancreatic tissues (scale bar = 10 μm) with quantitative scoring.. (F) The levels of serum inflammatory cytokines (TNFα, IL-1β, and IL-6) in control and CAE_AP mice. (G) IHC staining and scoring of TNFα and TNFR1 in pancreatic tissues in control and CAE_AP mice. (H) IHC staining and scoring of TNFα and TNFR1 expression in pancreatic tissues of control and pancreatic duct ligation-induced AP (LIG_AP) mice. (I) IHC staining and scoring of TNFα and TNFR1 in pancreatic tissues from sham-operated and L-arginine-induced AP (LIG_AP) groups. (J) Western blot analysis and quantification of TNFR1 protein expression in pancreatic tissues from control and cerulein-induced AP model mice. (K) Quantitative reverse transcription polymerase chain reaction (qRT-PCR) measurement of *Tnfa*and *Tnfrsf1a* transcript levels. (L) Enzyme-linked immunosorbent assay (ELISA) quantification of serum TNFα and TNFR1 levels in serum elevated in AP patients.; (M) Comparative analysis of TNFα and TNFR1 protein levels among healthy controls and AP patients stratified by disease severity. **P＜0.05＜**P＜0.01* and ****P＜0.001* were considered significant. Data were expressed as the means±SD. Data represent mean ± standard deviation (SD) of at least three independent experiments.

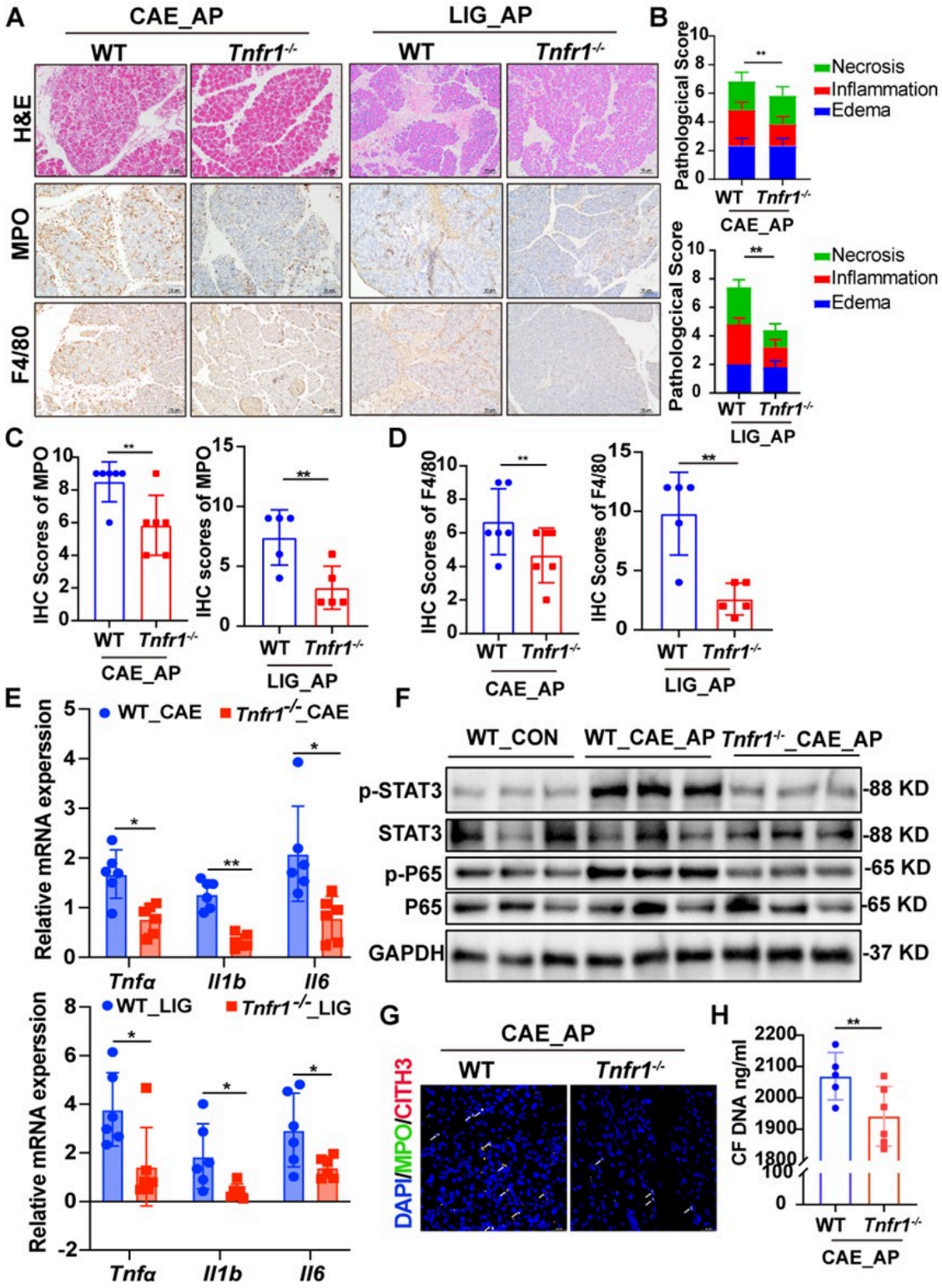


Figure 2

***Tnfrsf1a* deletion attenuates inflammatory responses in two acute pancreatitis (AP) animal models: cerulenin-induced (CAE_AP) and duct ligation (LIG_AP).** (A) Representative H&E and IHC analysis of pancreatic tissues from wild-type (WT) and *Tnfrsf1a* $^{-/-}$ mice following caerulein- or duct ligation-induced AP. H&E staining reveals tissue damage, while IHC detects neutrophil infiltration (myeloperoxidase, MPO) and macrophage accumulation (F4/80) (scale bar = 10 μm). (B) Quantitative scoring of pancreatic injury

severity (H&E-stained sections from A. (C, D) Quantitative assessment of MPO (neutrophils, C) and F4/80 (macrophages, D) by IHC scoring in caerulein - and duct ligation-induced AP models. (E) qRT-PCR analysis of inflammatory cytokine mRNA levels (*Il1b*, *Il6*, *Tnf*) in pancreatic tissues from WT and *Tnfrsf1a*$^{-/-}$ mice. (F) Western blot detection of P65, STAT3, and their phosphorylated forms (p-P65, p-STAT3) in pancreatic tissues from control or cerulein-induced AP mice (WT vs. *Tnfrsf1a* $^{-/-}$). (G) Immunofluorescence detection of neutrophil extracellular traps (NETs) via MPO (green) and citrullinated histone H3 (CitH3, red) co-localization. (H) Quantification of serum cell-free DNA (cfDNA, NETs marker) by fluorometric assay. Statistical significance was assessed by one-way ANOVA (for multi-group comparisons) or two-tailed Student's t-test (for two-group comparisons), with **P□0.05□**P□0.01* and ****P □0.001* considered significant. Data are presented as mean ± SD from three independent experiments.

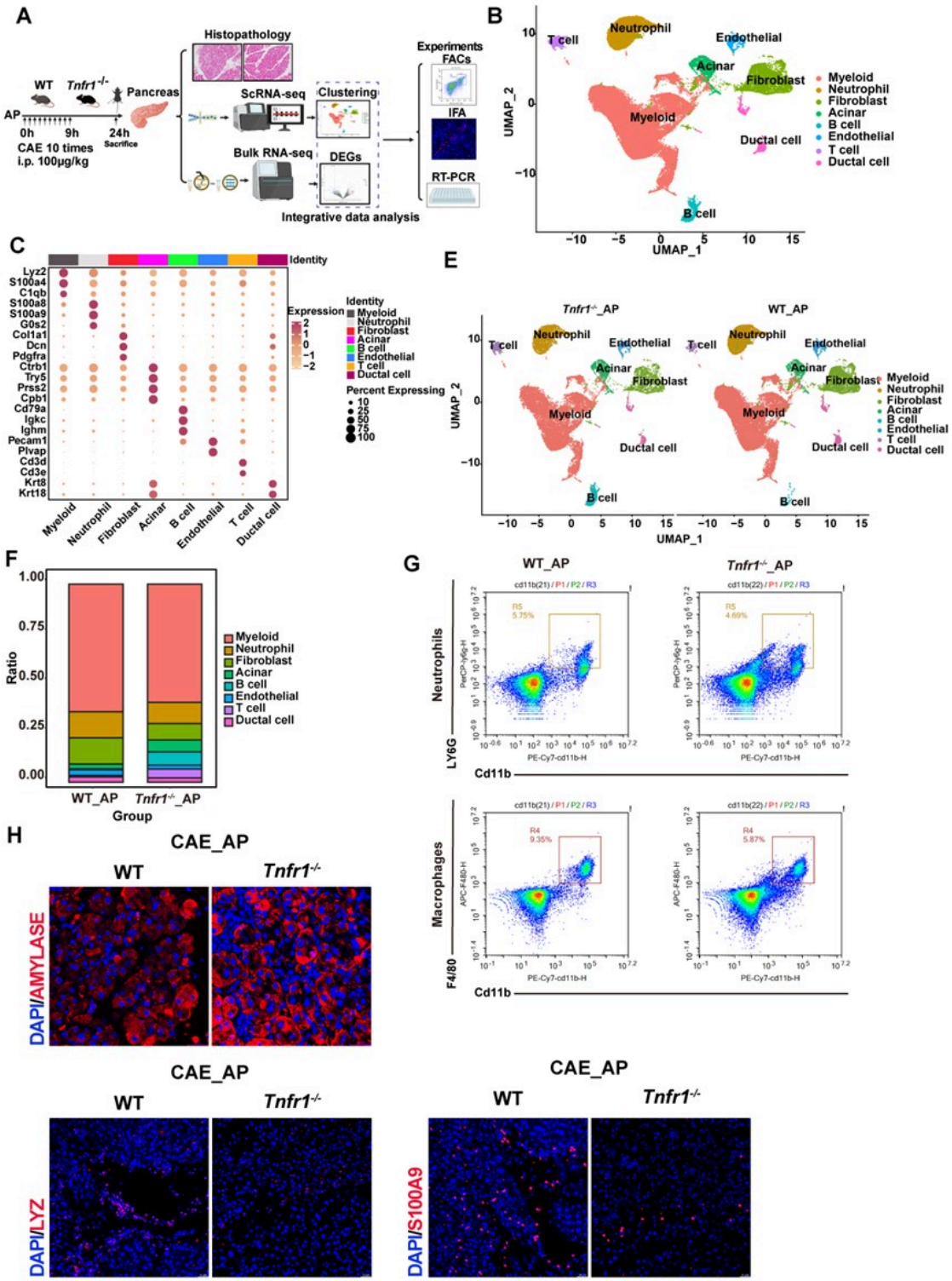


Figure 3

TNFR1 deficiency alters inflammatory cell profiles in acute pancreatitis revealed by single-cell RNA sequencing (scRNA-seq). (A) Schematic workflow of scRNA-seq experimental design and computational analysis pipeline. (B) Uniform Manifold Approximation and Projection (UMAP) visualization of all sequenced cells, colored by annotated cell type clusters (n = 52277). (C) Dot plot of lineage-defining marker genes across the 8 identified cell populations: dot size represents expression

prevalence; color indicates mean normalized expression. (D) UMAP plots stratified by genotype, highlighting differential cell distribution between WT and *Tnfrsf1a*$^{-/-}$ mice. (E) Stacked bars shoeing proportional abundance of each cell type in WT versus *Tnfrsf1a* $^{-/-}$ mice. (F) Flow cytometry quantification of pancreatic neutrophil (CD11b^{+}Ly6G^{+}) and macrophage (CD11b^{+}F4/80^{+}) frequencies. (G) Representative immunofluorescence images of pancreatic sections stained for acinar cells (Amylase^{+}, green), macrophages (Lyz^{+}, red), and neutrophils (S100A9^{+}, white). Nuclei counterstained with DAPI (blue; scale bar = 50 μm).

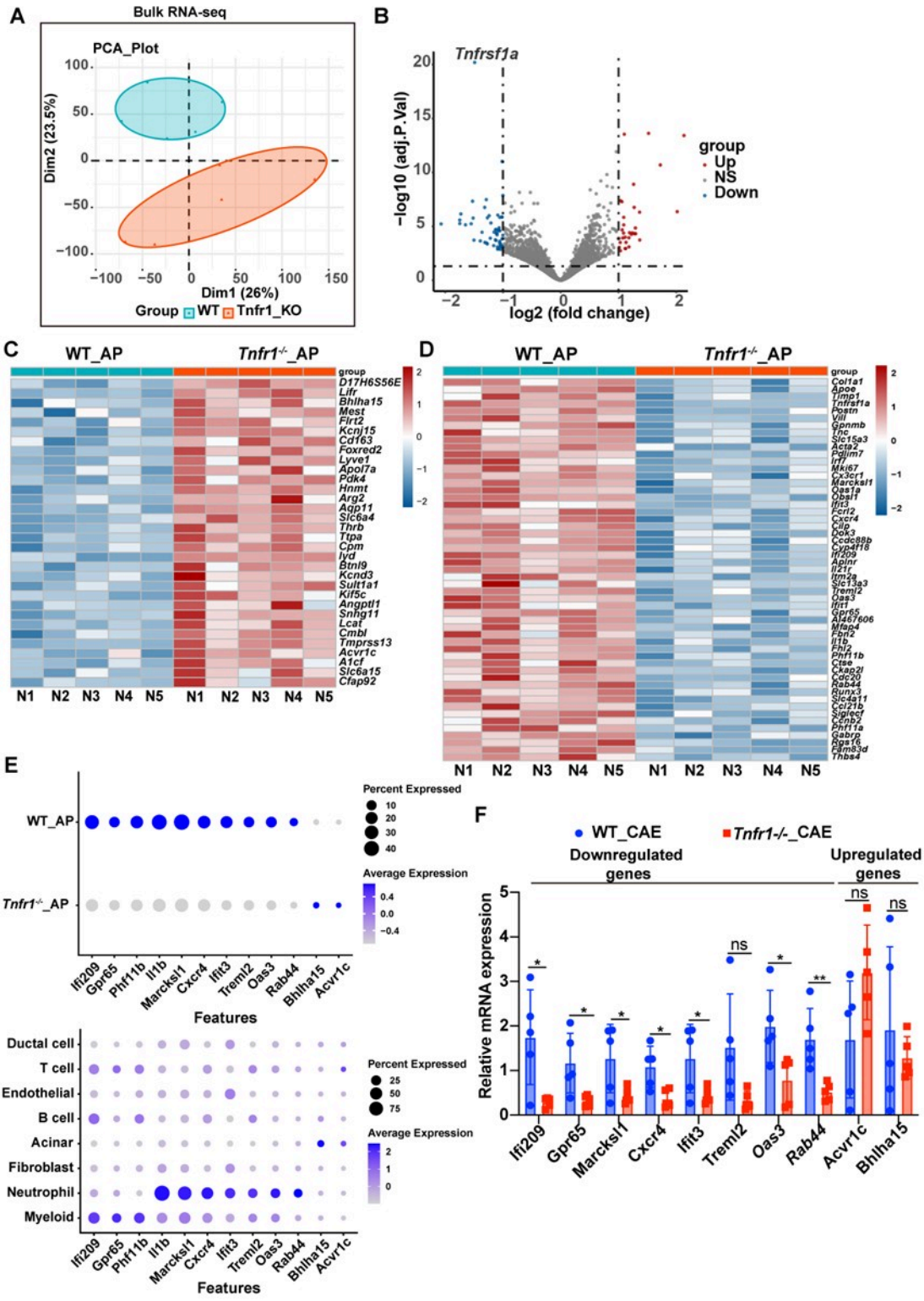


Figure 4

Multi-omics analysis identifies Tnfr1-dependent neutrophil/macrophage dysregulation and cytokine suppression. (A) Principal component analysis (PCA) of bulk RNA-seq data in WT and *Tnfrsf1a*$^{-/-}$ transcriptomes, illustrating genotype-driven clustering (WT vs. *Tnfrsf1a*$^{-/-}$). (B) Volcano plot of differentially expressed genes (DEGs: $\log_2$(fold change) ≥ 1, *P.adjust* < 0.05 between WT and *Tnfrsf1a*$^{-/-}$

mice, red highlights statistically significant DEGs. (C-D) Heatmaps of genotype-specific DEGs: *Tnfrsf1a*$^{-/-}$-upregulated genes (C), and *Tnfrsf1a*$^{-/-}$-downregulated genes (D) (Z-score normalized expression). (E) Dot plot of consensus DEG expression patterns from scRNA-seq (rows: prioritized genes; columns: cell clusters): dot size represents expression prevalence; color indicates mean normalized expression. (F) qRT-PCR validation of 11 prioritized DEGs in pancreatic tissues from WT and *Tnfrsf1a*$^{-/-}$ mice. **P□0.05□ **P□0.01* and ****P□0.001* were considered significant. Data are presented as mean ± SD from three independent experiments.

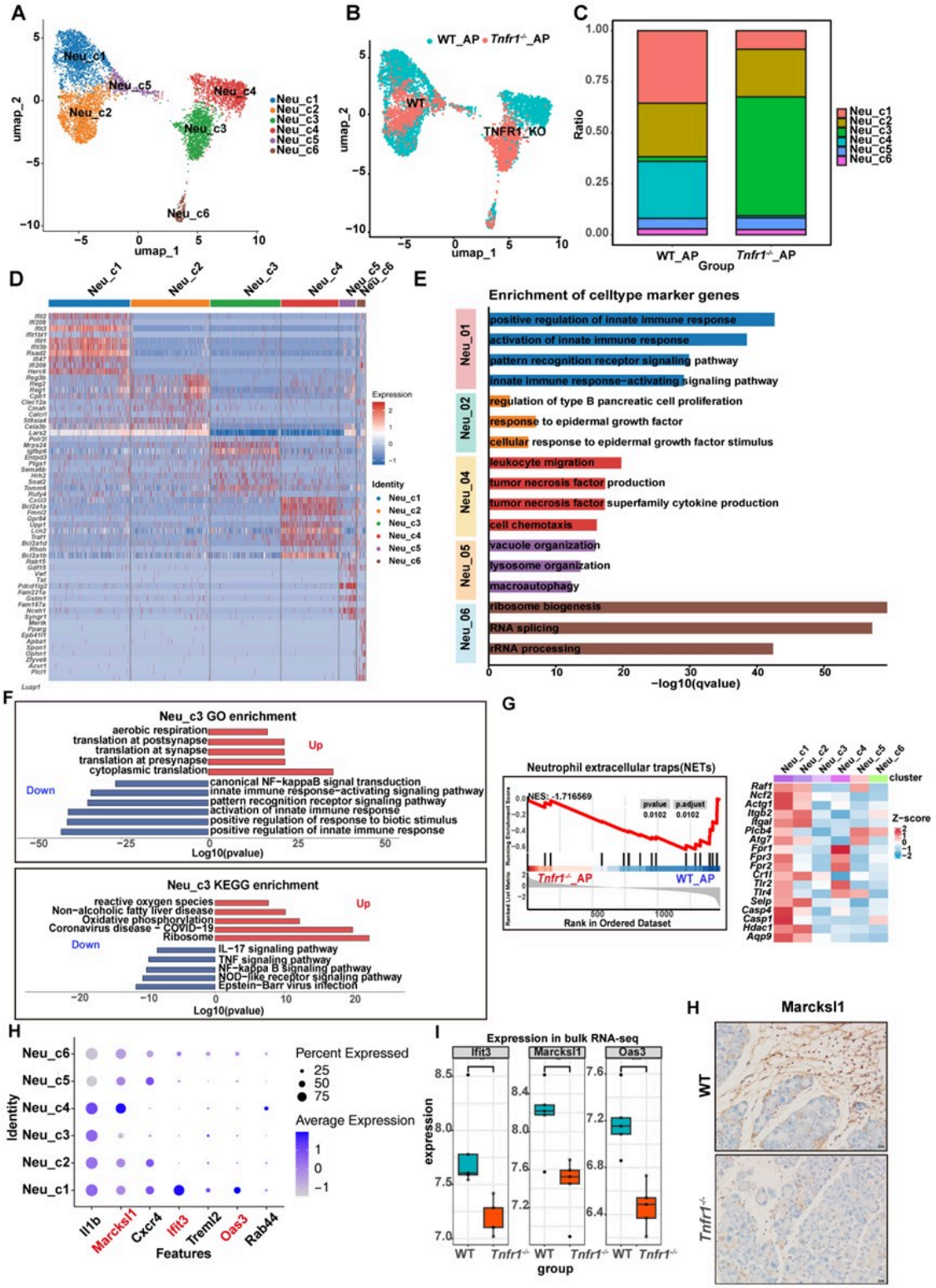


Figure 5

***Tnfrsf1a*$^{-/-}$ neutrophils exhibit reduced *Marcksl1/Ifit3/Oas3* expression and acquire inflammatory suppression properties. (A)** UMAP visualization of neutrophil subclusters from scRNA-seq data (colors denote subsets Neu_01-06). **(B)** Genotype-stratified UMAP plots of neutrophil subclusters between WT and *Tnfrsf1a*$^{-/-}$ mice. **(C)**

Quantification of neutrophil (Neu_01-06) subset proportions across genotypes. **(D)** Heatmap of top 10 marker genes for neutrophil subclusters. **(E)** GO term enrichment analysis of Neu_01/02/04/05/06 functional pathways. **(F)** Integrated GO/KEGG pathway analysis revealing inflammatory suppression functions of Neu_03. **(G) Neutrophil extracellular trap (NET) signatures.** ***Upper***: Heatmap of NETs-associated genes across subclusters; *Lower*: GSEA of NETs-related gene sets in WT vs. *Tnfr1*$^{-/-}$ neutrophils. **(H)** Expression dynamics of *Marcksl1*, *Ifit3*, *Oas3*, *Cxcr4*, *Treml2*, and *Rab44* across subclusters (dot size: detection rate; color: mean log-normalized expression) **(I)** Validation of *Marcksl1*, *Ifit3*, and *Oas3* expression via bulk RNA-seq (isolated neutrophils; mean ± SD; n=5) **(J)** Immunohistochemical quantification of MARCKSL1 protein. *Left*: Representative images (scale bar=50μm); *Right*: Blinded histoscore analysis. **P□0.05□**P□0.01* and ****P□0.001* were considered significant. Data were expressed as the means±SD.

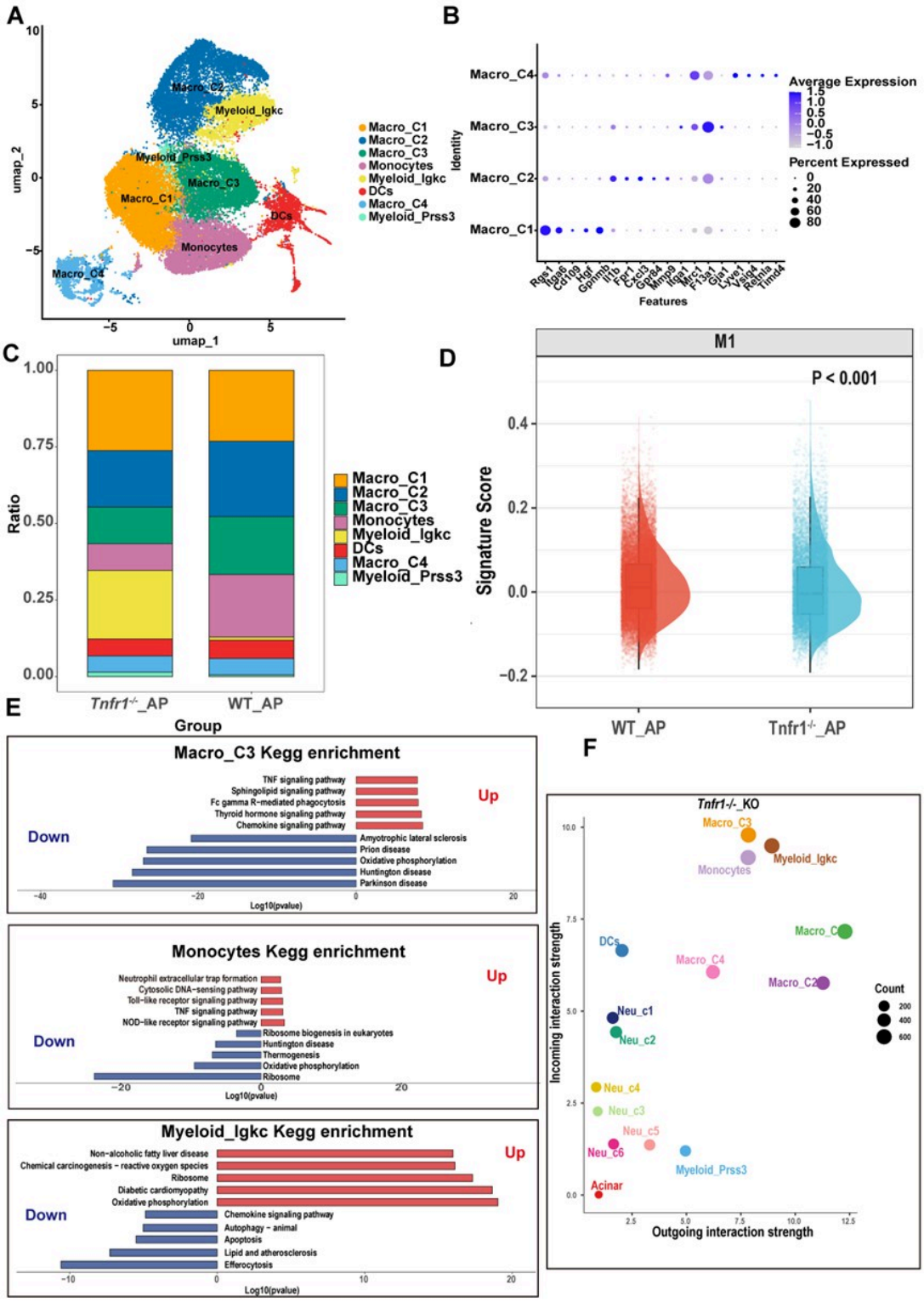


Figure 6

A *Tnfrsf1a*$^{-/-}$ dependent Myeloid_Igkc subpopulation attenuates inflammatory signaling in acute pancreatitis. (A) UMAP visualization of myeloid clusters from scRNA-seq data (colors: Macrophage/Monocyte subsets). (B) Dot plot of signature gene expression across 4 macrophage subsets (dot size: detection rate; color: Z-score). (C) Quantification of myeloid subset frequencies showing relative expansion of *Myeloid_Igkc* in *Tnfrsf1a*$^{-/-}$ mouse. (D) M1 score of WT_AP and *Tnfr1*$^{-/-}$_AP

group (E) KEGG pathway enrichment reveals distinct immunological functions: *Upper*: pro-inflammatory pathways in Macro_C3 and Monocytes; *Lower*: Inflammatory suppression signatures in Myeloid_Igkc. (F) Based on cell communication analysis (CellChat), the bubble plot shows the communication activity among acinar cells, neutrophils, and myeloid cell subpopulations.

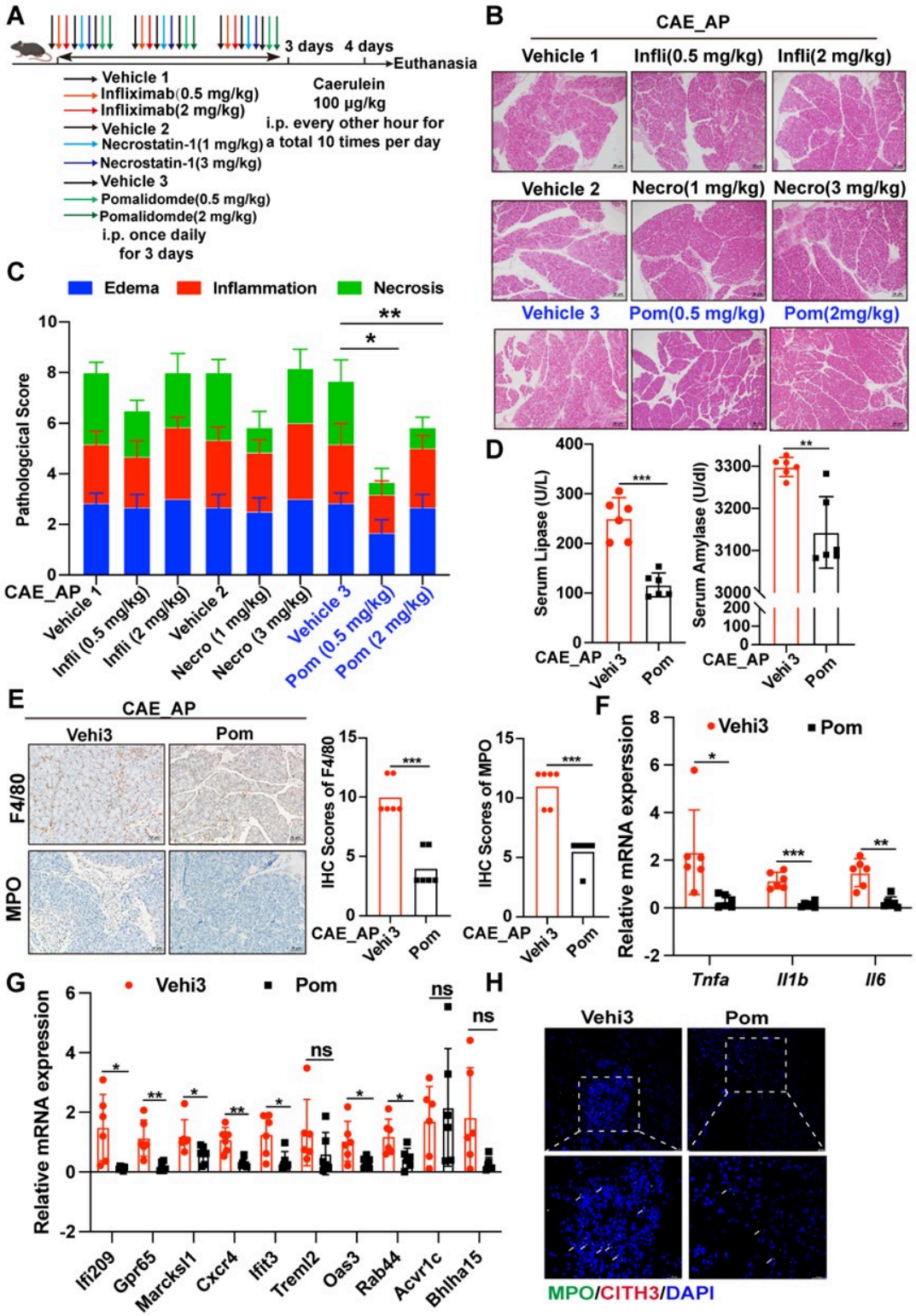


Figure 7

Three TNFα/TNFR1 pharmacological blockades attenuate inflammation and acinar damage in acute pancreatitis. (A) Treatment timeline: Mice received TNFα inhibitors (pomalidomide 0.5 mg/kg, etanercept 10 mg/kg, infliximab 5 mg/kg) or vehicle before cerulein-induced AP. Pomalidomide showed a promising effect. **(B)** Representative H&E-stained pancreatic sections from three inhibitor-treated groups and vehicle controls. **(C)** Histopathological scoring of pancreatic injury ((∑ edema/necrosis/inflammation; mean ± SD; *n*=6). **(D)** Serum amylase and lipase levels following pomalidomide optimization (0.5 mg/kg dose selected for downstream assays). **(E)** IHC analysis and quantification of MPO (left) and macrophage F4/80 infiltration (right). **(F)** qRT-PCR measurement of pancreatic inflammatory cytokines. **(G)** Expression profiling of neutrophil-associated genes (*Ifi209*, *Gpr65*, *Phf11b*, *Marcksl1*, *Cxcr4, Ifit3*, *Treml2*, *Oas3*, *Rab44*, *Bhlha15*, and *Acvr1c*) by qRT-PCR. **(H)** IF co-staining of MPO (green) and CitH3 (red) to assess NETs formation. **P□0.05□**P□0.01* and ****P□0.001* were considered significant. Data were expressed as the means±SD.

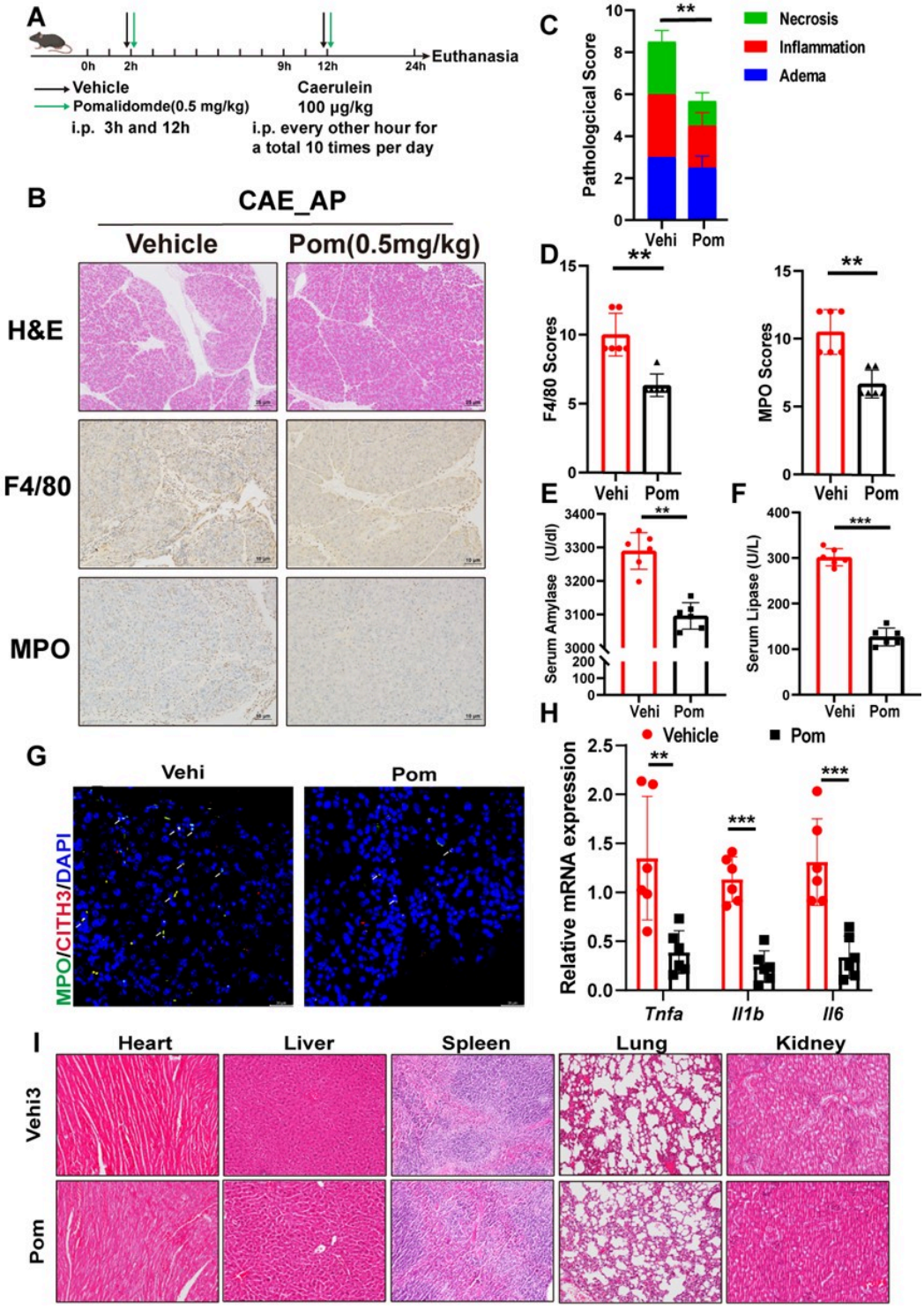


Figure 8

TNFα blockade after acute pancreatitis onset attenuates pancreatic injury. (A) Experimental timeline of cerulein-induced AP followed by intraperitoneal pomalidomide treatment (0.5 mg/kg i.p.). **(B)** Representative H&E-stained pancreatic sections from pomalidomide-treated and vehicle control mice. **(C)** Histopathological scoring of pancreatic injury severity (edema/necrosis/inflammation) **(D)** IHC scoring of MPO (left) and F4/80 (right) infiltration. **(E)** qRT-PCR validation of suppressed pancreatic

inflammatory cytokines (*Tnfα*, *Il-1β*, *Il-6*). **(F)** Serum amylase and lipase levels post-treatment. **(G)** IF co-staining of MPO (green) and CitH3 (red) demonstrating less NETs formation. **(I)** H&E staining of different organ between group Vechi3 and group POM. **P□0.05□**P□0.01* and ****P□0.001* were considered significant. Data were expressed as the means±SD.

Supplementary Files

This is a list of supplementary files associated with this preprint. Click to download.

- GAPDH22.tif
- TNFR1.tif
- GAPDH22.scnB.tif
- PP65.scnB.tif
- TNFR1.scnB.tif
- P65.scnB.tif
- GAPDH.scnB.tif
- TableS2Primers.xlsx
- P65.tif
- GAPDH.tif
- TableS1Antibodies.xlsx
- PP65.tif
- PSTAT3.scnB.tif
- TableS3DEGs.xlsx
- PSTAT3.tif
- STAT3.tif
- STAT3.scnB.tif
- Graphicalabstract.jpg
- Supplementaryfigures.docx